Geometric phase shaping of terahertz vortex beams.

Amalya Minasyan, Clément Trovato, Jérôme Degert, Eric Freysz, Etienne Brasselet, Emmanuel Abraham

Geometric phase shaping of terahertz vortex beams

Amalya Minasyan,[1] Clément Trovato,[1] Jérôme Degert,[1] Eric Freysz,[1] Etienne Brasselet,[1,2] and Emmanuel Abraham[1,*]

[1]Univ. Bordeaux, CNRS, LOMA, UMR 5798, F-33400 Talence, France
[2]e-mail: etienne.brasselet@u bordeaux.fr
*Corresponding author: emmanuel.abraham@u bordeaux.fr

We propose a topological beam-shaping strategy of terahertz (THz) beams using geometric phase elements made of space-variant birefringent slabs. Quasi-monochromatic THz vortex beams are produced and characterized both in amplitude and phase from the reconstructed real-time two-dimensional imaging of the electric field. Nonseparable superpositions of such vortex beams are also obtained and characterized by two-dimensional polarimetric analysis. These results emphasize the versatility of the spin-orbit electromagnetic toolbox to prepare on-demand structured light endowed with polarization-controlled orbital angular momentum content in the THz domain, which should find many uses in future THz technologies.

OCIS codes: (110.6795) Terahertz imaging; (080.4865) Optical vortices; (260.5430) Polarization; (060.5060) Phase modulation.

The unique properties of terahertz (THz) radiation, such as good penetration through various nonconductive materials, low scattering, free space propagation, low photon energy, and broad spectral bandwidth, encouraged the development of THz photonics [1]. More precisely, the initial developments of THz optics mainly consisted of engineer sources and detec tors, which subsequently implied the need for THz optical el ements such as lenses, splitters, polarizers, and retarders [2]. Nowadays, there is still plenty of room for technological im provements, for instance, regarding THz beam shaping. A par ticular situation corresponds to topological beam shaping that refers to tailor made structured fields endowed with phase and/ or polarization singularities. Such beams are now common in the visible domain and have already found a huge number of applications (e.g., in sensing, microscopy and astronomical im aging, trapping and manipulating of matter, information and communication technologies), whereas fewer works have been reported so far in the THz domain.

A basic ingredient of structured light corresponds to phase singularities (or "vortices") that are location in space, where the phase is undefined. Such singularities are locally described in a plane by a pure phase factor of the form $\exp(i\ell\varphi)$, with ℓ as an integer and φ as the usual azimuthal angle. Many techniques have been implemented to engineer beams carrying on axis phase singularities, usually called vortex beams, in the visible domain and, quite naturally, a straightforward strategy con sisted of performing mapping to the THz domain. One can mention the use of refractive three dimensional spiral phase plates, with an early demonstration in the sub THz domain 20 years ago [3], and more recent realizations covering the THz domain, for instance, at 0.3 THz [4], 0.62 THz [5], and in the range from 2 to 4 THz [6]. Flat THz vortex beam generators have also been realized, for instance, at 0.75 THz using an array of wavelength size V shaped antennas [7], at 0.31 THz [8], in the range from 1 to 1.6 THz [9], and at 2.1 THz [10] using a computer generated holograms.

Vector beams, which refer to light beams with space variant polarization states in the transverse plane, represent another kind of structured beam that has attracted interest in THz op tics. So far, the most studied cases are radially and azimuthally polarized beams. Radially polarized beams have been produced by using different kinds of radial polarizers, such as a tapered waveguide at 0.1 THz [11] and azimuthally patterned sub wavelength dichroic gratings in the range from 0.3 to 0.9 THz [12]. Concentric and radial antennas have been also proposed to generate radial and azimuthal polarization states, respectively, in the range from 0.5 to 2 THz [13]. On the other hand, various nonlinear processes have also been explored to generate THz vector beams [14–16]. Recently, the broadband generation of radially polarized THz beams has been shown in the range from 0.75 to 2 THz [17] by optical rectification of radially polarized near infrared pulses. Moreover, broadband THz vortex beams of topological charge $\ell = \pm 1$ have been extracted by selective polarization filtering of a generated poly chromatic THz vector beam [17].

Although various aspects of singular THz optics have been already explored, there is not yet a well established topological shaping approach enabling simple yet efficient generation of THz beams with arbitrary orbital angular momentum states. Here, we propose to exploit the geometric phase (see Ref. [18]

for an overview in the context of spin orbit interactions of light) in order to achieve polarization controlled THz vortex beams and superposition them from "regular" THz beams free from any singularities. This is done by using a single element, namely, a space variant birefringent slab endowed with an azimuthally varying in plane optical axis orientation. Indeed, this allows versatile interplay between the spin (polarization degree of freedom) and orbital (spatial degree of freedom) electromagnetic angular momentum. By doing so, this work extends to the THz domain's previous use of geometric phase optical elements [19] in the visible domain [20] and should find many uses in future THz technologies.

The experimental setup is presented in Fig. 1. An amplified Ti:Sapphire femtosecond laser source centered at an 800 nm wavelength with a 1 kHz repetition rate, 1.5 mJ pulse energy, and 50 fs pulse duration is split into pump and probe beams for THz field generation and detection. Regular broadband linearly polarized THz pulses over the typical range from 0.1 to 2.5 THz are prepared by optical rectification of amplified laser pulses in a (110) cut ZnTe nonlinear crystal [21], and a quasi monochromatic beam is obtained by placing a 1 THz bandpass filter (200 GHz full width at half maximum bandwidth) after the ZnTe crystal. Then, topological shaping of THz pulses basically relies on the use of a half wave quartz birefringent retarder whose optical axis orientation angle ψ in the transverse plane has the form $\psi = q\varphi$ (q half integer), as introduced in the framework of optical vortex generation in the visible domain [22]. The effect of such an optical element (often called a q plate) on an incident field can be easily grasped from the Jones calculation by applying the φ dependent Jones matrix $\mathbf{J}$ to an incident, fully polarized monochromatic plane wave described by the Jones vector $\mathbf{E}_{\text{in}}$. Indeed, neglecting diffraction, this gives an output field $\mathbf{E}_{\text{out}} = \mathbf{J} \cdot \mathbf{E}_{\text{in}}$, which is expressed on the (x, y) basis as

$$\mathbf{E}_{\text{out}} = \begin{pmatrix} \cos 2\psi & \sin 2\psi \\ \sin 2\psi & \cos 2\psi \end{pmatrix} \cdot \begin{pmatrix} a \\ b \end{pmatrix}, \qquad \textbf{(1)}$$

where the complex number (a, b) defines the incident polarization state. In this work, we consider two situations: (i) incident circular polarization, namely $(a, b) = (1/\sqrt{2})(1, i\sigma)$, where $\sigma = \pm 1$ refers to left/right polarization handedness and (ii) incident linear polarization, namely, $(a, b) = (\cos\theta, \sin\theta)$ where θ refers to polarization state azimuth. Without lack of generality, we restrict our study to the case $q = 1/2$, with the subsequent generalization to arbitrary values of q being straightforward. In addition, we practically use a 8 segmented half wave retarder for a 1 THz frequency made of quartz crystal (from Tydex; see Fig. 1), instead of a smoothly varying azimuthal profile for the angle ψ, which does not affect the results.

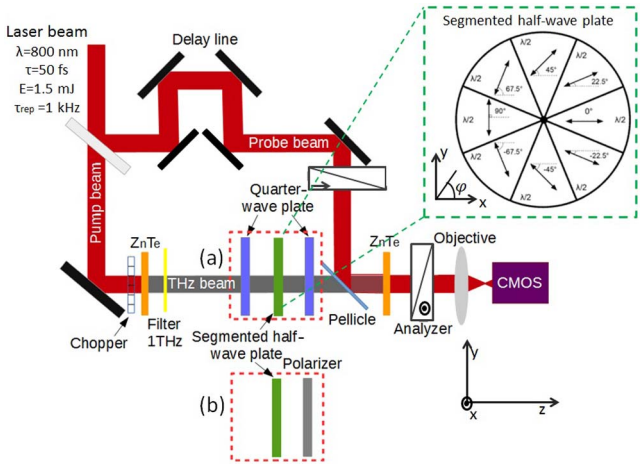

Fig. 1. Experimental setup for the generation and detection of THz vortex beams [case (i), see inset (a)] and THz vector beams [case (ii), see inset (b)]. See text for details.

The case (i) is carried out by preparing an incident circularly polarized THz beam with helicity σ, which is done by inserting a 1 THz quarter wave retarder after the bandpass filter [see inset (a) of Fig. 1]. One gets from Eq. (1)

$$\mathbf{E}_{\text{out}} = \frac{1}{\sqrt{2}} \begin{pmatrix} 1 \\ i\sigma \end{pmatrix} e^{i\sigma\varphi}, \qquad \textbf{(2)}$$

namely, a circularly polarized vortex beam with a helicity controlled topological charge $\ell = \sigma$. The real time generated THz vortex electric field is fully reconstructed in two dimensions using a pump probe detection scheme. This is made using a high speed 1 kHz CMOS camera coupled to an electro optical detection owing to a second (110) cut ZnTe crystal, where the THz beam and delayed probe laser pulse interact [23,24] via a second order nonlinear Pockels effect (see Fig. 1). The resulting image of the modulated probe light intensity is then read out on the camera, from which the time dependent THz electric field amplitude is deduced. Indeed, through the electro optic effect, the probe pulse experiences a polarization modulation that is proportional to the strength of the THz electric field. This polarization modulation is measured by sending the probe beam through an analyzer; then, an objective lens images the crystal plane onto the CMOS camera [25]. Note that the signal is obtained by setting the analyzed THz field polarization state to linear, which is made by placing another quarter wave retarder after the geometric phase element, which does not affect the sought after spiraling phase spatial distribution of Eq. (2). Images are acquired at a 500 Hz frame rate via dynamic subtraction of the background [26]. The signal to noise ratio is eventually improved by averaging 500 successive frames, which corresponds to a 1 s integration time. The temporal evolution of the THz electric field pulse is then reconstructed by controlling the time delay between the THz and probe pulses via an optical delay line (see Fig. 1). The results are presented in Fig. 2 for $\sigma = \pm 1$, where THz intensity transverse patterns are obtained by averaging the THz pulse intensity for different time delays [Figs. 2(a) and 2(b)]. Instantaneous amplitude transverse patterns are shown in Figs. 2(c) and 2(d) over half a THz period duration (i.e., $T \simeq 1$ ps, that is $\simeq$300 μm free space delay). As expected, the doughnut shaped intensity patterns shown in Figs. 2(a) and 2(b) are reminiscent of the on axis phase singularity that is associated with a value of zero of the THz intensity. On the other hand, the σ dependent spatiotemporal spiraling structure of the electric field shown in Figs. 2(c) and 2(d) corresponds to the presence of a phase singularity with a topological charge $\ell = \sigma$, since a σ dependent 2π rotation of the pattern per wavelength is observed. This can also be observed in the media file Visualization 1, in which the left part corresponds to $\sigma = +1$ [i.e., Fig. 2(d)] and the right part to $\sigma = -1$ [i.e., Fig. 2(c)].

It is noteworthy that the above spin controlled THz vortex generation does not require us to prepare incident THz pulses

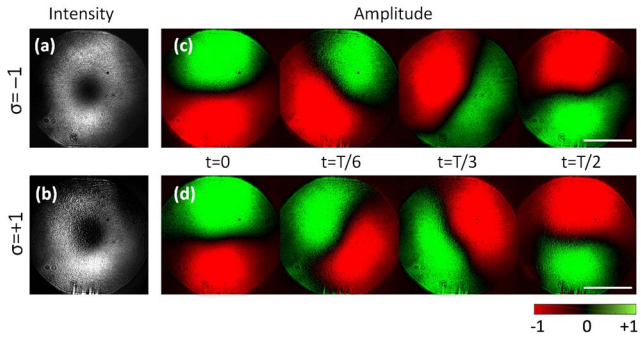

Fig. 2. (a) and (b) Intensity patterns of the 1 THz vortex beam ob tained in case (i) for $\sigma = \pm 1$. (c) and (d) Temporal evolution of the THz electric field transverse distribution revealing phase singularity of topological charge $\ell = \sigma$. Scale bar: 10 mm (see Visualization 1).

at 1 THz. Indeed, we can directly use the broadband THz pulses (0.1 2.5 THz), since the recorded data contain both the amplitude and phase information at all frequencies. This implies that transforming the temporal information into spec tral information can be numerically done by a fast Fourier transform. By doing so, the amplitude and phase spatial distri bution data are obtained for each frequency. A demonstration is illustrated in Fig. 3, where the intensity and phase transverse patterns at 1 THz extracted from the polychromatic data are shown in panels (a) and (b), respectively, for $\sigma = +1$. Again, one thus unambiguously concludes that the generation of a spin controlled unit charge THz vortex, whose linear azimuthal dependence of the phase along the circle line in Fig. 3(a) is quantitatively shown in Fig. 3(c), is in good agree ment with the theory, $\Phi = \sigma\varphi$. In addition, we note that a broadband THz vortex could be easily obtained by mere use of achromatic quarter wave retarders instead of monochromatic ones; however, this would be at the expense of the overall vortex generation efficiency. Indeed, the frequency dependent Jones matrix $\mathbf{J}(\nu)$ is expressed as

$$\mathbf{J} = \begin{pmatrix} \cos\frac{\Delta}{2} + i\,\sin\frac{\Delta}{2}\,\cos\,2\psi & i\,\sin\,2\psi\,\sin\frac{\Delta}{2} \\ i\,\sin\,2\psi\,\sin\frac{\Delta}{2} & \cos\frac{\Delta}{2} \quad i\,\sin\frac{\Delta}{2}\,\cos\,2\psi \end{pmatrix}, \tag{3}$$

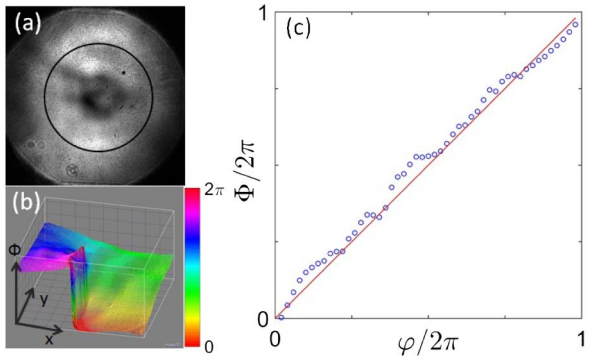

Fig. 3. Intensity (a) and phase (b) distributions of the generated vortex beam at 1 THz extracted from the polychromatic field proc essed by the geometric phase vortex generator where $\sigma = +1$; see text for details. (c) Azimuthal angle dependence of the phase along the circle line shown in panel (a). Markers: experimental data. Solid line: theory.

where $\Delta(\nu) = \pi\nu/\nu_0$ is the frequency dependent birefringent phase retardation, ν_0 being the frequency associated with half wave retardance, here with $\nu_0 = 1$ THz, which assumes frequency independent birefringence, which is a fair approxi mation. One thus gets

$$\mathbf{E}_{\text{out}} = \frac{1}{\sqrt{2}}\left[\cos\frac{\Delta}{2}\begin{pmatrix}1\\ i\sigma\end{pmatrix} + i\,\sin\frac{\Delta}{2}\begin{pmatrix}1\\ i\sigma\end{pmatrix}e^{i\sigma\varphi}\right], \tag{4}$$

which shows that the σ polarized output component carries a phase singularity with topological charge $\ell = \sigma$ whatever the frequency ν, up to a frequency dependent intensity modulation factor $\sin^2[\pi\nu/(2\nu_0)]$. Then, any quantity of interest when dealing with vortex generation from polychromatic fields can be readily derived from the latter expression.

Then we explore the case (ii), which is done by preparing an incident linearly polarized THz beam with an azimuth angle θ. One gets from Eq. (1)

$$\mathbf{E}_{\text{out}} = \begin{pmatrix}\cos(\varphi \quad \theta)\\ \sin(\varphi \quad \theta)\end{pmatrix}, \tag{5}$$

namely, a vector beam characterized by an inhomogeneous lin ear polarization state having an azimuth angle $\Psi = \varphi \quad \theta$. In particular, a radially polarized beam is expected when $\theta = 0$, whereas an azimuthally polarized beam is expected when $\theta = \pi/2$. In practice, THz vector beam generation is demon strated from the spatially resolved azimuth angle Ψ of the electric field. From the definition $\Psi = \arctan(E_y/E_x)$, it is therefore enough to place a linear polarizer after the segmented half wave retarder, as shown in inset (b) of Fig. 1, and to image the vertical and horizontal output beam electric field compo nents, E_y and E_x. For the individual measurements of E_x and E_y, the polarization of the laser probe beam was kept horizon tal, and, for a given position of the THz polarizer, the ZnTe detection crystal was rotated in order to maximize the electro optical signal. The corresponding data are shown in Figs. 4(a) and 4(b) for $\theta = 0$ and Figs. 5(a) and 5(b) for $\theta = \pi/2$, from which the Ψ map is evaluated, as shown in Figs. 4(c) and 5(c). We note that such a direct determination of the electric field orientation is an option that one cannot afford in the visible region of the near infrared domain, where the electric field vec tor can hardly be measured. In both cases, we observe a total increase of 2π of the polarization azimuth angle ψ. Moreover, this angle is equal to 0 if the polar angle φ is 0 or $\pi/2$, respec tively, for radial and azimuthal beams. Finally, the angular dependence of polarization azimuths for radial and azimuthal beams along the circle lines in Figs. 4(c) and 5(c) are plotted in Figs. 4(d) and 5(d). They are in good agreement with theoreti cal linear fits. Distributions of polarization vectors are recon structed from the polarization azimuth angle values for radial and azimuthal beams, as shown in the insets of Figs. 4(d) and 5(d), respectively.

Interestingly, the approach by Imai *et al.* that consists of extracting a vortex beam from a vector beam by projection onto a circular polarization state [17] can be grasped by rewriting Eq. (5) as

$$\mathbf{E}_{\text{out}} = \frac{1}{2}\left[\begin{pmatrix}1\\ i\end{pmatrix}e^{-i\varphi} \pm \begin{pmatrix}1\\ i\end{pmatrix}e^{i\varphi}\right], \tag{6}$$

where the ± sign refers to $\theta = (0, \pi/2)$. Indeed, this corre sponds to a nonseparable spin orbit state (i.e., neither the polarization nor the spatial degree of freedom can be factorized)

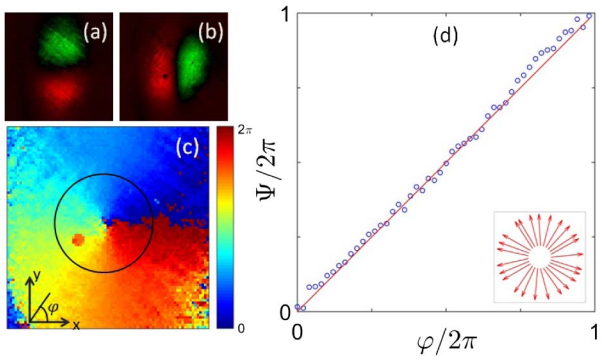

Fig. 4. Analysis of radially polarized THz beam ($\theta = 0$). Transverse distributions of the vertical (E_y) and horizontal (E_x) electric field components are shown in panels (a) and (b), respectively. (c) Spatial distribution of the azimuth angle $\Psi = \arctan(E_y/E_x)$. (d) Dependence of the polarization azimuth Ψ of the radial vector beam: circles, experimental data along the circle line shown in panel (c). Markers: experimental data; Solid line: theory.

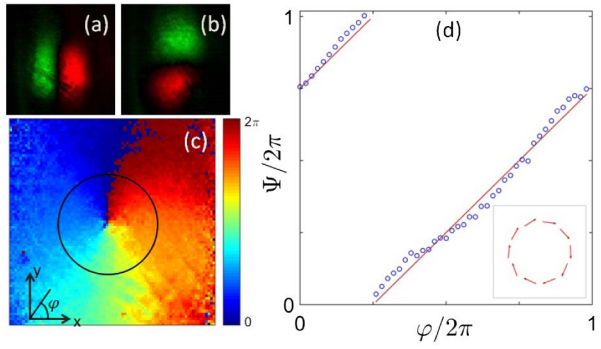

Fig. 5. Analysis of azimuthally polarized THz beam ($\theta = \pi/2$). Panel descriptions are similar to those of Fig. 4.

that consists of the superposition of contra circularly polarized vortex fields with opposite unit topological charges. circular polarization filtering of this electric field will thus give a vortex beam with a topological charge $\ell = \sigma$. In our case, where the birefringent phase retardation is $\Delta = \pi$, we have access either to spin controlled THz vortex beams or azimuth controlled THz vector beams without need for post polarization filtering. The broadband features merely depend on the use of achromatic retarders, which is not a serious technological issue. Moreover, the present demonstration in the particular case where $q = 1/2$ can be straightforwardly generalized to any half integer value of the parameter q, which would lead to the generation of THz vortex beams with topological charge $\ell = 2\sigma q$ in the case (i) and THz vector beams of order $\ell = 2q$ in the case (ii), similar to what happens in the well documented visible domain.

In conclusion, THz vortex beams and vector beams were generated using geometric phase elements. A high speed CMOS camera combined with EO detection was used to characterize the beams by employing a simple and direct measurement of the THz electric field. The possibility of generating broadband vortex beams with adapted optical elements and their characterization by means of a fast Fourier transform was also shown. Finally, we note recent theoretical developments toward alternative nonlinear strategies to generate THz twisted beams [27,28], calling for experimental demonstrations. This is likely to complement the present linear spin orbit THz toolbox to prepare on demand structured light endowed with polarization controlled orbital angular momentum content.

Funding. Agence Nationale de la Recherche (ANR) (ANR 10 IDEX 03 02).

Acknowledgment. This study has been carried out with financial support from the French State, managed by the French National Research Agency (ANR) in the frame of "the Investments for the future" Programme IdEx Bordeaux LAPHIA.

REFERENCES

1. P. Jepsen, D. Cooke, and M. Koch, Laser Photon. Rev. **5**, 124 (2011).
2. R. A. Lewis, J. Phys. D **47**, 374001 (2014).
3. G. Turnbull, D. Robertson, G. Smith, L. Allen, and M. Padgett, Opt. Commun. **127**, 183 (1996).
4. X. Wei, C. Liu, L. Niu, Z. Zhang, K. Wang, Z. Yang, and J. Liu, Appl. Opt. **54**, 10641 (2015).
5. X. Wang, J. Shi, W. Sun, S. Feng, P. Han, J. Ye, and Y. Zhang, Opt. Express **24**, 7178 (2016).
6. K. Miyamoto, K. Suizu, T. Akiba, and T. Omatsu, Appl. Phys. Lett. **104**, 261104 (2014).
7. J. He, X. Wang, D. Hu, J. Ye, S. Feng, Q. Kan, and Y. Zhang, Opt. Express **21**, 20230 (2013).
8. J. Salo, J. Meltaus, E. Noponen, M. M. Salomaa, A. Lönnqvist, T. Koskinen, V. Viikari, J. Säily, J. Häkli, J. Ala Laurinaho, J. Mallat, and A. V. Räisänen, J. Opt. A **4**, S161 (2002).
9. Z. Xie, X. Wang, J. Ye, S. Feng, W. Sun, T. Akalin, and Y. Zhang, Sci. Rep. **3**, 3347 (2013).
10. B. A. Knyazev, Y. Y. Choporova, M. S. Mitkov, V. S. Pavelyev, and B. O. Volodkin, Phys. Rev. Lett. **115**, 163901 (2015).
11. T. Grosjean, F. Baida, R. Adam, J. P. Guillet, L. Billot, P. Nouvel, J. Torres, A. Penarier, D. Charraut, and L. Chusseau, Opt. Express **16**, 18895 (2008).
12. X. Wang, S. Wang, Z. Xie, W. Sun, S. Feng, Y. Cui, J. Ye, and Y. Zhang, Opt. Express **22**, 24622 (2014).
13. S. Winnerl, B. Zimmermann, F. Peter, H. Schneider, and M. Helm, Opt. Express **17**, 1571 (2009).
14. C. D'Amico, A. Houard, M. Franco, B. Prade, A. Mysyrowicz, A. Couairon, and V. T. Tikhonchuk, Phys. Rev. Lett. **98**, 235002 (2007).
15. G. Chang, C. J. Divin, C. H. Liu, S. L. Williamson, A. Galvanauskas, and T. B. Norris, Opt. Lett. **32**, 433 (2007).
16. R. Imai, N. Kanda, T. Higuchi, Z. Zheng, K. Konishi, and M. Kuwata Gonokami, Opt. Express **20**, 21896 (2012).
17. R. Imai, N. Kanda, T. Higuchi, K. Konishi, and M. Kuwata Gonokami, Opt. Lett. **39**, 3714 (2014).
18. K. Y. Bliokh, F. J. Rodriguez Fortuno, F. Nori, and A. V. Zayats, Nat. Photonics **9**, 796 (2015).
19. R. Bhandari, Phys. Rep. **281**, 1 (1997).
20. L. Marrucci, E. Karimi, S. Slussarenko, B. Piccirillo, E. Santamato, E. Nagali, and F. Sciarrino, J. Opt. **13**, 064001 (2011).
21. A. Rice, Y. Jin, X. F. Ma, X. C. Zhang, D. Bliss, J. Larkin, and M. Alexander, Appl. Phys. Lett. **64**, 1324 (1994).
22. L. Marrucci, C. Manzo, and D. Paparo, Phys. Rev. Lett. **96**, 163905 (2006).
23. G. Gallot and D. Grischkowsky, J. Opt. Soc. Am. B **16**, 1204 (1999).
24. Q. Wu, M. Litz, and X. C. Zhang, Appl. Phys. Lett. **68**, 2924 (1996).
25. Z. Jiang, X. G. Xu, and X. C. Zhang, Appl. Opt. **39**, 2982 (2000).
26. F. Miyamaru, T. Yonera, M. Tani, and M. Hangyo, Jpn. J. Appl. Phys. **43**, L489 (2004).
27. K. Saito, T. Tanabe, and Y. Oyama, Appl. Opt. **54**, 2769 (2015).
28. T. Wakayama, T. Higashiguchi, H. Oikawa, K. Sakaue, M. Washio, M. Yonemura, T. Yoshizawa, J. S. Tyo, and Y. Otani, Sci. Rep. **5**, 9416 (2015).